

# Acoustic measurement of the Deepwater Horizon Macondo well flow rate

Richard Camilli<sup>a,1</sup>, Daniela Di Iorio<sup>b</sup>, Andrew Bowen<sup>a</sup>, Christopher M. Reddy<sup>c</sup>, Alexandra H. Techet<sup>d</sup>, Dana R. Yoerger<sup>a</sup>, Louis L. Whitcomb<sup>a,e</sup>, Jeffrey S. Seewald<sup>c</sup>, Sean P. Sylva<sup>c</sup>, and Judith Fenwick<sup>a</sup>

<sup>a</sup>Department of Applied Ocean Physics and Engineering, Woods Hole Oceanographic Institution, Woods Hole, MA 02543; <sup>b</sup>Department of Marine Sciences, University of Georgia, Athens, GA 30602; <sup>c</sup>Department of Marine Chemistry and Geochemistry, Woods Hole Oceanographic Institution, Woods Hole, MA 02543; <sup>d</sup>Department of Mechanical Engineering, Massachusetts Institute of Technology, Cambridge, MA 02139; and <sup>e</sup>Department of Mechanical Engineering, Johns Hopkins University, Baltimore, MD 21218

Edited\* by Marcia K. McNutt, US Geological Survey, Reston, VA, and approved August 11, 2011 (received for review January 25, 2011)

**O**n May 31, 2010, a direct acoustic measurement method was used to quantify fluid leakage rate from the *Deepwater Horizon* Macondo well prior to removal of its broken riser. This method utilized an acoustic imaging sonar and acoustic Doppler sonar operating onboard a remotely operated vehicle for noncontact measurement of flow cross-section and velocity from the well's two leak sites. Over 2,500 sonar cross-sections and over 85,000 Doppler velocity measurements were recorded during the acquisition process. These data were then applied to turbulent jet and plume flow models to account for entrained water and calculate a combined hydrocarbon flow rate from the two leak sites at seafloor conditions. Based on the chemical composition of end-member samples collected from within the well, this bulk volumetric rate was then normalized to account for contributions from gases and condensates at initial leak source conditions. Results from this investigation indicate that on May 31, 2010, the well's oil flow rate was approximately  $0.10 \pm 0.017 \text{ m}^3 \text{ s}^{-1}$  at seafloor conditions, or approximately  $85 \pm 15 \text{ kg s}^{-1}$  ( $7.4 \pm 1.3 \text{ Gg d}^{-1}$ ), equivalent to approximately  $57,000 \pm 9,800$  barrels of oil per day at surface conditions. End-member chemical composition indicates that this oil release rate was accompanied by approximately an additional  $24 \pm 4.2 \text{ kg s}^{-1}$  ( $2.1 \pm 0.37 \text{ Gg d}^{-1}$ ) of natural gas (methane through pentanes), yielding a total hydrocarbon release rate of  $110 \pm 19 \text{ kg s}^{-1}$  ( $9.5 \pm 1.6 \text{ Gg d}^{-1}$ ).

Gulf of Mexico | oil spill | buoyant plume | buoyant jet | subsurface

**A**ccurate assessment of the hydrocarbon fluid release rate from well blowouts such as that of the *Deepwater Horizon* Macondo well provides fundamental information for evaluating intervention options to regain well control, properly scaling oil collection and containment operations, estimating the total spill volume, assessing environmental damage, and investigating well casing or blowout preventer (BOP) failure modes. On May 31, 2010, a direct acoustic technique was used to measure the volumetric flow rate of fluids (liquid and gas) emitted from the *Deepwater Horizon* Macondo well. This method, which adapts acoustic techniques previously developed for deep-sea hydrothermal vent research (1), enabled observation from a remotely operated vehicle (ROV) (Fig. S1) at horizontal standoff distances of between 2 and 7 m, providing a noncontact method of measurement wherein the sensors did not disturb the flow or become fouled with oil or gas hydrate accretions. Despite the optical opacity of the fluid, this acoustic technique enabled quantitatively detailed measurement of the leaks' cross-sectional areas and velocity profiles. This acoustic flow rate assessment was conducted on a "not to interfere basis" due to the well containment operations being carried out from late April through mid-July. Data were thus collected on an opportunistic basis during short time intervals between containment procedures.

Acoustic measurement commenced immediately following the unsuccessful "top kill" attempt, before the riser was removed and the lower marine riser package Top Hat #4 containment system was placed on top of the BOP. At this time the well's

leaks were located in two distinct areas: a kinked section of the riser pipe immediately above the BOP's flex joint ( $28.7381^\circ \text{ N}$   $88.3660^\circ \text{ W}$ ), and at the broken end of the riser approximately 225 m north-northwest of the well's BOP. Independent acoustic measurements were required at each site.

## Results

Horizontal cross-section images of fluids flowing from the well were recorded above each of the leak locations using the imaging sonar (1,089 cross-section images at  $3.0 \pm 0.1 \text{ m}$  above the broken riser source, and 1,500 cross-section images  $1.3 \pm 0.1 \text{ m}$  above the BOP-kink source), requiring between 3 and 4 min of acquisition per leak site (Fig. 1). To aid these operations, the ROV was equipped with a pair of parallel-sighting lasers that assisted in aiming the imaging sonar and Doppler sonar at the centers of the hydrocarbon leaks (Fig. S1). Cross-section area calculation was based on interframe motion tracking of acoustic returns using a standard threshold of 3.5 dB (signal-to-noise ratio of 1.5:1) or more above background noise (2), and flow areas were counted only if the contiguous area was equal to or greater than  $0.01 \text{ m}^2$ . The threshold for contiguous region was defined as an area larger than the Nyquist theorem limit of the imaging sonar's pixel resolution at a range of approximately 7 m. Using this method, the mean cross-section areas of the leak jets of the broken riser and BOP kink are  $1.10$  and  $0.996 \text{ m}^2$ , respectively, with the standard error of the mean for each leak site of  $\pm 0.005$  and  $\pm 0.004 \text{ m}^2$  (equivalent to  $\pm 0.45$  and  $\pm 0.42\%$  relative standard error), respectively. Optical observation of flow width using the parallel-sighting lasers (0.1-m beam spacing) indicates that the acoustic cross-section values are valid (Fig. S2). The ROV's high-definition video camera was, however, uncalibrated and did not account for optical distortions, making it inappropriate for quantitatively precise size estimation.

At each of the two leak sites, the ROV was positioned facing the rising source fluids with vehicle headings of  $120^\circ$ ,  $240^\circ$ , and  $360^\circ$ . Doppler sonar data were obtained with the ROV holding station in a fixed position within 0.5 m of a desired positional set point at each station for durations of approximately 5 min. The flow velocity data from a  $60^\circ$  upward pointing Doppler beam (Fig. S3) were postprocessed and combined with ROV navigation position estimates to compute the instantaneous vertical velocity for each ping ensemble within a 3D coordinate frame. The

---

Author contributions: R.C., D.D., A.B., D.R.Y., and L.L.W. designed research; R.C., A.B., C.M.R., and S.P.S. performed research; R.C., D.D., A.B., C.M.R., A.H.T., D.R.Y., L.L.W., and J.S.S. contributed new reagents/analytic tools; R.C., D.D., A.B., C.M.R., A.H.T., D.R.Y., L.L.W., J.S.S., S.P.S., and J.F. analyzed data; and R.C., D.D., A.B., C.M.R., A.H.T., D.R.Y., L.L.W., and J.F. wrote the paper.

The authors declare no conflict of interest.

\*This Direct Submission article had a prearranged editor.

'To whom correspondence should be addressed. E-mail: rcamilli@whoi.edu.

This article contains supporting information online at [www.pnas.org/lookup/suppl/doi:10.1073/pnas.1100385108/DCSupplemental](http://www.pnas.org/lookup/suppl/doi:10.1073/pnas.1100385108/DCSupplemental).

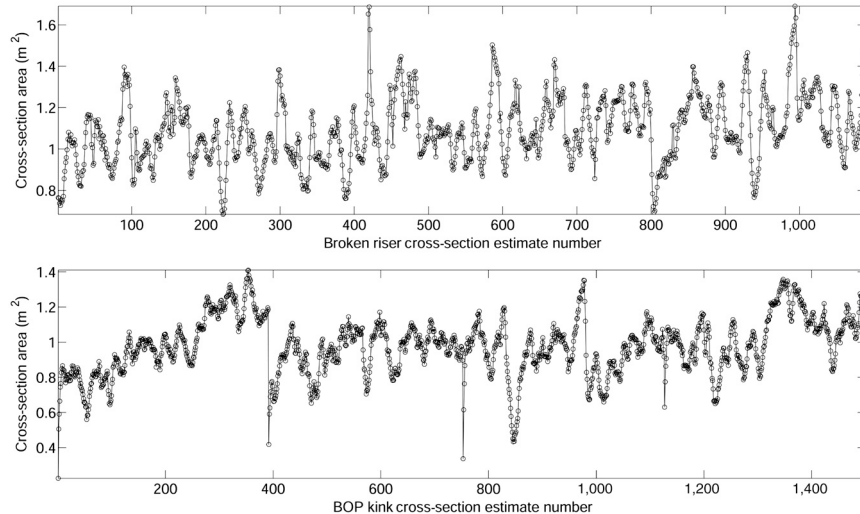


**Fig. 1.** Measured jet cross-section areas based on imaging sonar using motion tracking with a 3.5 dB (signal-to-noise ratio = 1.5:1) threshold at a horizontal plane 3 m above the broken riser leak source (*Upper*), and 1.3 m above the BOP-kink leak source (*Lower*). X-axis values denote the sample number, with a total of 1098 cross-section measurements taken for the broken riser leak and 1,500 cross-section measurements for the BOP kink. Measurements were recorded at a rate of approximately 6 Hz, for durations of 3 min at the broken riser site, and 4 min at the BOP-kink site. The periodic variability in cross-section areas for each of the leak sites is consistent with turbulent flow.

velocity calculations are based on an initial set of 42,270 broken riser and 42,894 BOP-kink Doppler sonar measurements.

The momentum length scale,  $L_M$ , of the jet sources, was approximately 0.6 m for the broken riser and 0.1 m for the BOP kink (*SI Text*). The differing source sizes and geometries may have influenced the length scale, with the BOP-kink leak site being made up of numerous small diameter sources acting as diffusers, whereas the broken riser was comprised of a single large diameter source. In comparison, the  $L_M$  of deep-sea hydrothermal vent flows are at most 1 m (3). Based on the estimated momentum length scales, Doppler measurements at both sites were determined to be within the region of buoyancy-driven plume flow, as characterized by Papanicolaou and List (4). The BOP-kink imaging sonar cross-section plane was determined to be within the plume region, whereas the broken riser cross-section plane was within the upper limits of its jet flow region.

With these flow correspondences, the perimeter of fluid flow at each leak site is defined using the cross-section area of the imaging sonar measurement and augmented by empirically derived expansion rates of 0.108 and 0.105 (4) for jet and plume flow, respectively, where the horizontal radius of fluid flow,  $b_w$ , expands upward or contracts downward in the plume flow region as  $b_w \sim 0.105z$ , where  $z$  is the vertical distance from the sonar imaging plane and  $b_w$ , similarly expands upward or contracts downward in the jet flow region as  $b_w \sim 0.108z$ . Downward continuing the expansion models from the measured cross-section planes to their respective sources predict a source diameter of  $0.53 \pm .02$  m for broken riser, and a  $0.84 \pm .02$  m effective source diameter for the multiple closely spaced leak orifices at BOP-kink site.

ROV video imagery showed that the broken riser orifice was modestly deformed but maintained a generally circular shape and that the multiple BOP-kink leaks were arranged in a pattern that approximated an oval (5). Consequently, flow rates were determined using accepted models of free round jets emanating into a quiescent fluid and transitioning to buoyancy-driven plumes (4, 6, 7). Under these models, at sufficient distance from the orifice the flow becomes fully developed. Within this region, the velocity profiles become self-similar and the initial jet velocity profile at the orifice becomes inconsequential (8, 9). A distance,  $z_c$ , corresponding to 5 times the orifice diameter, is typically considered sufficient for fully developed flow.

Raw Doppler measurements within the plume volumes reveal negative (downward) velocities with maximum magnitude approaching that of positive (upward) velocities (Figs. 2 and 3), symptomatic of intense turbulence. Optical imagery shows turbulent mixing well fluids rapidly transitioning to fine emulsions of hydrocarbons and water (*Fig. S2*) that are visually indistinguishable from the emulsion layer described at approximately 1,100- to 1,300-m depth (10).

Using the previously described buoyancy-driven plume expansion model, velocity measurements recorded at varying heights within this control volume are downward-continued to a plane common with the cross-section plane (*SI Text*).

Downward-continued vertical velocity measurements within the broken riser and BOP-kink plume measurement volumes indicate normal distributions about their means, with respective median values of  $0.11$  and  $1.4 \times 10^{-4}$  m s $^{-1}$ . When binned at equally spaced intervals along their respective axial radii, the downward-continued vertical velocities are highest at the axial center, transitioning to lower velocities as a function of radial distance from the center, generally following a 2D Gaussian distribution about the centerline (Fig. 3). The spatially and temporally averaged vertical velocity,  $w_{avg}$ , at the cross-section plane height for the broken riser and BOP kink are, respectively,  $0.14$  and  $0.05$  m s $^{-1}$ . Standard error values for these vertical velocity estimates are, respectively,  $\pm 0.003$  and  $\pm 0.008$  m s $^{-1}$  (equivalent to  $\pm 2$  and  $\pm 16\%$  relative standard error).

Volumetric fluid flow rate (well fluids and entrained seawater),  $\mu$ , is computed at the cross-section plane height as the product of the cross-sectional area multiplied by its respective  $w_{avg}$ , yielding  $0.154 \pm 0.004$  m $^3$  s $^{-1}$  for the broken riser and  $0.050 \pm 0.008$  m $^3$  s $^{-1}$  for the BOP kink. Entrained seawater,  $Q_{water}$ , is estimated for the cross-section plane as a function of the flow's lateral surface area,  $A_{lat}$ , extending between the source and cross-section plane (6),  $w_{avg}$ , and an entrainment coefficient (4),  $\alpha$ , where  $\alpha_{jet} = 0.0535 \pm 0.0025$  is used for the broken riser site, and  $\alpha_{plume} = 0.0833 \pm 0.0042$  is used for the BOP-kink site (*SI Text*). Based on calculated  $A_{lat}$  surface areas of  $8.1 \pm 0.17$  and  $4.0 \pm 0.27$  m $^2$  for the broken riser jet and BOP-kink plume, respectively, and their associated  $w_{avg}$  velocities, the water entrainment rate at the cross-section planes are  $0.057 \pm 0.006$  and  $0.016 \pm 0.004$  m $^3$  s $^{-1}$ , respectively. These water volume entrainment values compare favorably to dilution estimated as a dimensionless function of distance from the jet orifice (7).

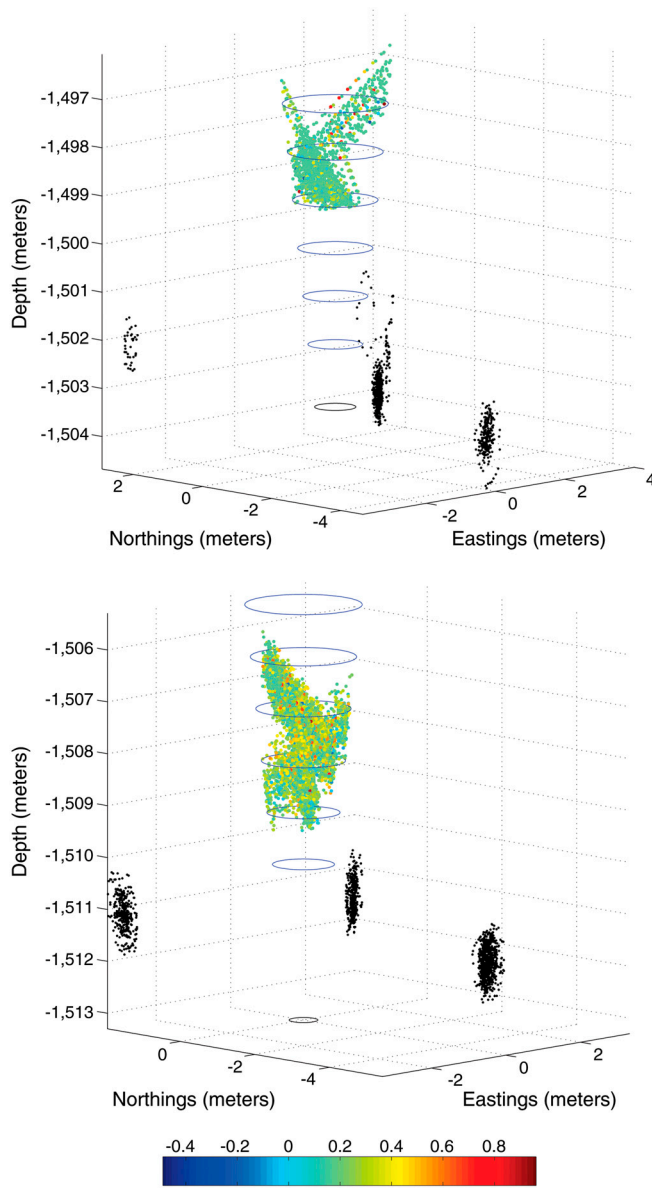


**Fig. 2.** Three-dimensional reconstruction of velocity fields based on Doppler sonar velocity field measurements recorded at the BOP-kink leak site (*Upper*) and the broken riser leak site (*Lower*). Each colored dot represents the location of a Doppler ping ensemble, with the dot color describing the estimated velocity in meters per second (as specified in the colorbar). The black ellipse in each graph indicates the calculated size and location of the leak source; blue dashed ellipses indicate the calculated flow perimeters. Black dots indicate the position of the ROV-mounted Doppler sonar during measurement.

The net volumetric fluid flux rates from the Macondo well leak sites,  $Q$ , are obtained by subtracting  $Q_{\text{water}}$  from  $\mu$ . Calculated  $Q$  values are thus  $0.097 \pm 0.011 \text{ m}^3 \text{ s}^{-1}$  for the broken riser leak and  $0.034 \pm 0.009 \text{ m}^3 \text{ s}^{-1}$  for the BOP-kink leak, yielding a combined well flux rate of approximately  $0.131 \pm 0.02 \text{ m}^3 \text{ s}^{-1}$ .

The volumetric well fluid-to-seawater mixing ratios at the broken riser and BOP-kink cross-section planes indicate that the ambient seawater entrained with the well fluids caused rapid cooling of these jets. Based on the ambient seawater temperature of  $4.4^\circ\text{C}$  (10), a maximum measured temperature of  $37^\circ\text{C}$  at a well fluid exit vent (11), and the specific heat of crude oil being approximately half that of seawater, the bulk fluid temperature of the BOP-kink jet was less than  $14^\circ\text{C}$  and the bulk fluid temperature of the jet at the broken riser cross-section plane is calculated

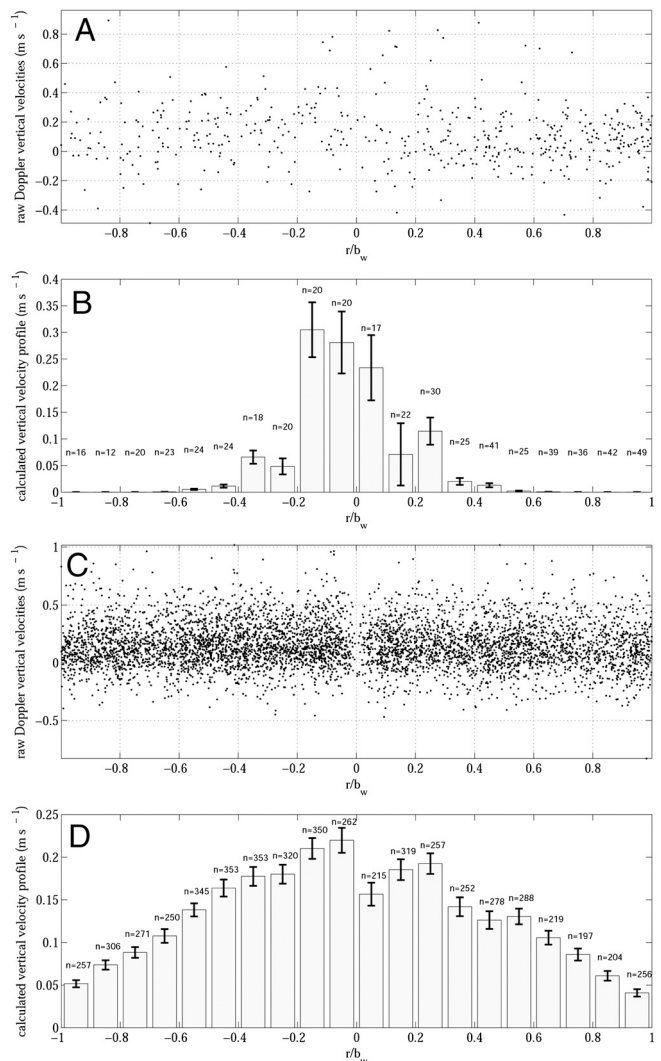


**Fig. 3.** Vertical velocity profiles of flow at the BOP kink and broken riser. *A* shows the raw vertical velocities for all recorded heights within the BOP plume measurement volume, *B* shows the calculated velocity profile at BOP-kink cross-section measurement plane using the downward-continued plume model. Velocities are binned at equally spaced intervals of  $0.1 r/b_w$ , where  $-r/b_w$  is the region recorded between the ROV and the jet's vertical axis, and  $+r/b_w$  is the distal region opposite  $-r/b_w$ . The number of measurements recorded within each bin is described as  $n$ , and error bars represent the standard error of the mean for each bin. *C* shows the raw vertical velocities for all recorded heights within the broken riser flow measurement volume, and *D* shows the calculated velocity profile at the broken riser cross-section measurement plane using the downward-continued plume model.

to have been less than  $13^\circ\text{C}$ , although the actual temperature at the broken riser source was presumably lower due to conductive cooling during well fluid transport within the several hundred meters of coiled riser pipe linking the BOP to the broken riser end location.

End-member chemical composition analysis by Reddy et al. (11) reveals that the well fluids contained no detectable formation water and were by mass approximately 15% methane, 7% ethane through pentanes, 77% hexanes and higher petroleum hydrocarbons, and less than 1% carbon dioxide and nitrogen (overall error  $\pm 2\%$ ). Thermodynamic calculations indicate that under initial source conditions ethane and higher hydrocarbons would remain in liquid form, suggesting that gas phase components would be limited to methane, carbon dioxide, and nitrogen.

Based on nonideal gas compressibility and a methane hydrate stability point of approximately  $15.5^\circ\text{C}$  at ambient hydrostatic

pressure (approximately 150 atm), the water that became turbulently entrained with the jet subjected these free gases to aqueous dissolution while simultaneously causing carbon dioxide to condense into liquid phase and transitioning methane into a hydrate phase. Under these conditions the well fluids at the cross-section plane heights were by volume 76% oil (i.e., hexanes and higher hydrocarbons), with the remaining fluid balance composed of methane hydrate, liquefied ethane through pentanes, and non-hydrocarbon gases.

Multiplying the estimated  $Q$  of each leak source with the calculated oil fraction,  $0.76 \pm 0.02$ , yields a net oil flow rate,  $Q_{\text{oil}}$ , of  $0.074 \pm 0.0096$  and  $0.026 \pm 0.0077 \text{ m}^3 \text{s}^{-1}$  of oil from the broken riser and BOP kink, respectively, for a combined total of  $0.10 \pm 0.017 \text{ m}^3 \text{s}^{-1}$ . Socolofsky et al. (12) estimated an oil density at ambient seafloor conditions of  $858 \text{ kg m}^{-3}$ , indicating a combined oil transport of approximately  $85 \pm 15 \text{ kg s}^{-1}$  (or  $7.4 \pm 1.3 \text{ Gg d}^{-1}$ ) from the two leak sites. Measured oil density was  $821 \text{ kg m}^{-3}$  at surface conditions (11), indicating that the volumetric oil flux rate calculated at ambient seafloor conditions would expand by 4.5% at surface conditions to approximately  $0.104 \pm 0.018 \text{ m}^3 \text{s}^{-1}$ , equivalent to  $57,000 \pm 9,800$  barrels of oil per day. As indicated by the end-member chemical composition (11), this oil release rate was accompanied by an additional  $24 \pm 4.2 \text{ kg s}^{-1}$  ( $2.1 \pm 0.37 \text{ Gg d}^{-1}$ ) of natural gas (methane through pentanes) from the two leak sites, yielding a total hydrocarbon release rate of  $110 \pm 19 \text{ kg s}^{-1}$  ( $9.5 \pm 1.6 \text{ Gg d}^{-1}$ ).

## Discussion

Although the overall statistical measurement error is inclusive of recorded natural variability in the turbulent flow, the methods described here may be subject to additional nonstatistical uncertainty caused by systematic observational or model biases. The extremely limited opportunity for data collection at the leak sites did not permit additional investigation. Nonetheless, comparison of measurement data with theoretical bounds and other independent measurements provide some indication of model performance and potential biases.

The sonar-derived source diameter calculations derived from average measured flow cross-section and distance-dependent jet flow expansion are in close agreement with other independent measurements. The broken riser source diameter, calculated at  $0.53 \pm 0.02 \text{ m}$ , is nearly identical to the nominal  $0.492 \text{ m}$  (19.375 in.) internal diameter of the *Deepwater Horizon* riser pipe (13, 14). Similarly, the sonar estimated BOP-kink source diameter, at  $0.84 \pm 0.02 \text{ m}$ , matches the maximum measured distance between individual leak orifices at the flattened riser section of the BOP kink (5).

Fluid velocity measurement errors due to ROV vehicle motions were calculated for each station. The ROV's mean X, Y, and Z component velocities during acoustic flow measurements were, respectively,  $-0.00009$ ,  $0.00016$ , and  $0.00023 \text{ m s}^{-1}$  for the broken riser site, and  $-0.00122$ ,  $-0.0015$ , and  $-0.00056 \text{ m s}^{-1}$  for the BOP-kink site. These measured mean vehicle velocities are negligible in comparison to the measured fluid flow velocities.

Unlike shallow water releases of oil and natural gas, which tend to generate two phase flow with a large initial density deficit and bubble slip velocities (15), the ambient seafloor pressure and temperature regime at the Macondo well site impose a minimum initial gas phase density of at least approximately  $120 \text{ kg m}^{-3}$  and an initial bulk (oil and gas) fluid density within a factor of two of the ambient seawater. Moreover, entrainment of the low temperature seawater indicates rapid density increases through cooling and phase transformations of methane and carbon dioxide, evolving the fluids into a single phase before the turbulent jet flow is fully developed. These near-source effects increase the bulk fluid density to approximately  $950 \text{ kg m}^{-3}$ , sharply eroding the initial density deficit and associated buoyancy forces (16). Optical imagery at each of the leak sites confirmed methane hydrate

formation within the near-field measurement volumes, indicating that the well fluids had rapidly cooled to a temperature of  $15.5^\circ\text{C}$  or less. Atmospheric observations in the vicinity of the well site also show that methane did not reach the sea surface (17, 18), and subsurface chemical measurements reveal that the methane instead formed a neutrally buoyant plume at approximately 1,100-m depth (10, 19), indicating that buoyancy-driven methane flux ceased within the initial 400 m of vertical water column transport.

Horizontal water currents measured in the vicinity of the well were less than  $0.08 \text{ m s}^{-1}$  (10), indicating that the horizontal water currents did not significantly influence the leaks' flow regimes and plume spreading rates within the length scales of the measurement regions. The minimum height,  $z_B$ , at which horizontal water column currents would cause the flow to bend horizontally and increase the lateral expansion rate as a result of horizontal momentum entrainment were at least an order of magnitude greater than the measurement volumes' vertical length scales (SI Text). Optical imagery recorded during ROV inspection of the leak sites confirmed that source fluids flowed along vertical axes to heights of substantially more than 10 m without any discernible lateral deviation above their respective source locations.

The calculations described here make use of the well's end-member chemical composition, which has an appreciably lower natural gas mass fraction than those reported from surface containment vessels (20) or from samples collected from within a leak source jet (11). If the source jet sample composition (11) is instead applied, the volume fraction of oil would decrease from  $0.76$  to  $0.68$ . This would decrease the net oil flux rate by approximately 11%, while simultaneously increasing the natural gas fraction (methane through pentanes) by an equivalent percentage.

The single day acoustic flow rate estimate reported here corresponds with other independently determined oil release estimates (21–23). The acoustic flow rate estimate may be used in conjunction with these independent well flow rate estimates from other dates to characterize potential release rate variability due to factors such as reservoir depletion and modification of the well structure during containment operations (24). As an ensemble, these estimates suggest a modestly decreasing trend in the well's flow rate as a function of time. If, however, this May 31, 2010, acoustic flow rate estimate of  $57,000 \pm 9,800$  barrels of oil per day is extrapolated as a static rate for the interval following the Macondo well blowout and continuing until well shut-in, it indicates a total release of  $4,800,000 \pm 800,000$  barrels of oil ( $0.81 \pm 0.1 \text{ Tg}$  total hydrocarbons) from the Macondo well from April 20, 2010, to July 14, 2010. Net oil leak to the ocean, calculated as this cumulative release, minus the oil collected using the riser insertion tube tool (25), Top Hat #4, and BOP choke and kill lines (20), totals approximately  $4,000,000 \pm 800,000$  barrels.

Considering that there existed no industry-accepted technologies for measuring hydrocarbon flow rate from this leaking deepwater well (26, 27), the acoustic methods described here provide a useful means for quantitative assessment of leakage rate. Prior to removal of the riser, the Macondo well's optically opaque, initially multiphase fluids and multiple irregularly shaped source jets (5) introduced a level of complexity that made flow estimation with optical methods difficult. Although this acoustic method requires integration of specialized hardware, it permitted a three-dimensional view through these fluids enabling highly resolved measurements of cross-sections and characterization of velocity fields within these complex flow regimes. Future deepwater well failure assessment efforts should include a portfolio of techniques that account for the physical and chemical complexity of the leak as well as mobilization requirements.

## Methods

These acoustic measurement methods were undertaken using a work-class ROV (Maxximum, Oceaneering International) that was specifically equipped by the authors for these operations with a dual-frequency identification sonar (DIDSON 3000 imaging sonar, Sound Metrics) and a 1.2-MHz acoustic Doppler sonar (acoustic Doppler current profiler, 1,200-kHz Workhorse, Teledyne RD) for direct measurement of the well fluid expulsion cross-sections and velocity distributions, respectively (Figs. S1 and S3).

The position and orientation of acoustic measurements were obtained by combining data from the ROV's standard suite of navigation sensors. The ship's survey (*MSV Ocean Intervention III*) provided 1-Hz position estimates of an ROV acoustic beacon, as reported by the ultrashort baseline (USBL) navigation system on the vessel (Sonardyne USBL, with integrated survey by Fugro Chance Inc.). These navigation estimates were augmented with 10-Hz heading, pitch, and roll of the ROV recorded by its inertial navigation system (Meridian Gyrocompass, Teledyne TSS). ROV depth was measured using a quartz depth sensor (Digiquartz®, Paroscientific). The vehicle's relative motion was also obtained from a Doppler velocity log (DVL) (300-kHz Navigator, Teledyne RD Instruments) operated in bottom-lock mode and recorded at 4 Hz. The USBL, orientation, and DVL data were processed using a complementary filter that combines the low-frequency content of the USBL position with the high-frequency content of the relative position from the DVL (28), (break frequency 0.002 Hz). In instances where the USBL position was unreliable (possibly due to interference from the leak sources or other vehicles operating in the area), an estimate of the distance to the jet flow was used to transform the DVL's relative displacements into a relative coordinate frame.

The sonar imaging plane was located  $3.0 \pm 0.1$  m above the broken riser source and  $1.3 \pm 0.1$  m above the BOP-kink source, with the imaging sonar transducer located at a horizontal distance of between 4 and 7 m from the leak sources (Fig. S3). These imaging sonar cross-section measurements were recorded using a 1.8-MHz acoustic frequency and with an acquisition rate of

1. Rona PA, et al. (2006) Entrainment and bending in a major hydrothermal plume, Main Endeavour Field, Juan de Fuca Ridge. *Geophys Res Lett* 33:L19313, 10.1029/2006GL027211.
2. Sound Metrics Corp. (2010) *DIDSON V5.25 Software Manual* (Sound Metrics Corp., Lake Forest Park, WA) p 81.
3. Speer KG (1999) Thermocline penetration of buoyant plumes. *Mid-Ocean Ridges, Dynamics of Processes Associated with Creation of New Ocean Crust*, eds JR Cann, H Elderfield, and A Laughton (Cambridge Univ Press), pp 249–263.
4. Papanicolaou PN, List E (1988) Investigations of round vertical turbulent buoyant jets. *J Fluid Mech* 195:341–391.
5. Kusek J (2010) *DH Riser Kink Holes—Measurement with Field Drawings and Image* (US Coast Guard Research and Development Center, New London, CT) p 14.
6. Morton B, et al. (1956) Turbulent Gravitational Convection from Maintained and Instantaneous Sources. *Proc R Soc Lond A Math Phys Sci* 234(1196):1–23.
7. Fischer HB, et al. (1979) *Mixing in Inland and Coastal Waters* (Academic, San Diego) p 483.
8. Pope SB (2000) *Turbulent Flows* (Cambridge Univ Press, New York) p 771.
9. Hinze JO (1975) *Turbulence* (McGraw-Hill, New York) p 790.
10. Camilli R, et al. (2010) Tracking hydrocarbon plume transport and biodegradation at Deepwater Horizon. *Science* 330:201–204.
11. Reddy CM, et al. (2012) Composition and fate of gas and oil released to the water column during the Deepwater Horizon oil spill. *Proc Natl Acad Sci USA* 109:20229–20234.
12. Socolofsky S, et al. (2012) Formation dynamics of subsurface hydrocarbon intrusions following the Deepwater Horizon blowout. *Geophys Res Lett* 38:L09602, 10.1029/2011GL047174.
13. Transocean (2010) Deepwater Horizon fact sheet, available from [http://www.deepwater.com/fw/filemanager/fm\\_file\\_manager\\_download.asp?FileName=Deepwater\\_Horizon\\_spec\\_sheet.pdf&FilePath=/\\_filelib/FileCabinet/Horizon/](http://www.deepwater.com/fw/filemanager/fm_file_manager_download.asp?FileName=Deepwater_Horizon_spec_sheet.pdf&FilePath=/_filelib/FileCabinet/Horizon/) (accessed December 30, 2010).
14. Vetcogray (2008) *HMF Marine Drilling Riser Coupling product information sheet*, available from [http://hydrilpressurecontrol.com/\\_pdf/pressureControlBrochures/VG\\_hmf\\_marine\\_drc.pdf](http://hydrilpressurecontrol.com/_pdf/pressureControlBrochures/VG_hmf_marine_drc.pdf) (accessed February 27, 2011).
15. Milgram JH (1983) Mean flow in round bubble plumes. *J Fluid Mech* 133:345–376.
16. Cardoso SSS, McHugh ST (2009) Turbulent plumes with heterogeneous chemical reaction on the surface of small buoyant droplets. *J Fluid Mech* 642:49–77.
17. Yvon-Lewis SA, et al. (2012) Methane flux to the atmosphere from the Deepwater Horizon oil disaster. *Geophys Res Lett* 38:L01602, 10.1029/2010GL045928.
18. Ryerson TB, et al. (2012) Atmospheric emissions from the Deepwater Horizon spill constrain air-water partitioning, hydrocarbon fate, and leak rate. *Geophys Res Lett* 38:L07803, 10.1029/2011GL046726.
19. Valentine DL, et al. (2010) Propane respiration jump-starts microbial response to a deep oil spill. *Science* 330:208–211.
20. US Department of Energy (2010) *Combined Total Amount of Oil and Gas Recovered Daily from the Top Hat and Choke Line Oil Recovery Systems* (US Department of Energy, Washington, DC).
21. National Commission on the BP Deepwater Horizon Oil Spill and Offshore Drilling (2010) *The Amount and Fate of the Oil—Draft—Staff Working Paper No. 3* (National Commission on the BP Deepwater Horizon Oil Spill and Offshore Drilling, Washington, DC) p 29.
22. Crone TJ, Tolstoy M (2010) Magnitude of the 2010 Gulf of Mexico oil leak. *Science* 330 (6004):634–634.
23. McNutt MK, et al. (2012) *Assessment of Flow Rate Estimates for the Deepwater Horizon/Macondo Well Oil Spill. Flow Rate Technical Group Report to the National Incident Command, Interagency Solutions Group* (US Department of Interior, Reston, VA) p 22.
24. Bristol S (2010) Government estimates—Through August 01 (Day 104). *Deepwater Horizon MC252 Gulf Incident Oil Budget* (National Oceanic and Atmospheric Administration, Silver Spring, MD).
25. US Department of Energy (2010) *Oil and Gas Recovery Data from the Riser Insertion Tube from May 17 until the Riser Insertion Tube Was Disconnected on May 24 in Preparation for Cutting Off the Riser*.
26. McKay L (2010) Congressional Hearing Testimony, Deepwater Horizon: Oil Spill Prevention and Response Measures and Natural Resource Impacts, House Transportation and Infrastructure Committee, May 19, 2010, Washington, DC.
27. Harris R (2010) “Gulf Spill May Far Exceed Official Estimates” (interview with BP Spokesman Bill Salvin), *Morning Edition: May 14, 2010* (National Public Radio).
28. Whitcomb LL, et al. (2000) Advances in underwater robot vehicles for deep ocean exploration: Navigation, control, and survey operations. *Robotics Research-The Ninth International Symposium* (Springer, London).